

ATOMIC LAYER DEPOSITION FOR EMERGING THIN-FILM MATERIALS AND APPLICATIONS

Epitaxial growth of $\text{Mg}_x\text{Ca}_{1-x}\text{O}$ on 4H-SiC(0001) and $\beta\text{-Ga}_2\text{O}_3(\bar{2}01)$ wide band gap semiconductors with atomic layer deposition

Xiabing Lou^{1,b),c)}, Xian Gong^{2,b)} , Sang Bok Kim¹, Roy G. Gordon^{3,a)}

¹Department of Chemistry and Chemical Biology, Harvard University, Cambridge, Massachusetts 02138, USA

²John A. Paulson School of Engineering and Applied Sciences, Harvard University, Cambridge, Massachusetts 02138, USA

³Department of Chemistry and Chemical Biology, John A. Paulson School of Engineering and Applied Sciences, Harvard University, Cambridge, Massachusetts 02138, USA

^{a)}Address all correspondence to this author. e-mail: gordon@chemistry.harvard.edu

^{b)}These authors contributed equally to this work.

^{c)}Present addresses: Cambridge Electronics Inc., 501 Massachusetts Avenue, Cambridge, MA 02139, USA

Received: 9 September 2019; accepted: 18 November 2019

SiC and Ga_2O_3 are promising wide band gap semiconductors for applications in power electronics because of their high breakdown electric field and normally off operation. However, lack of a suitable dielectric material that can provide high interfacial quality remains a problem. This can potentially lead to high leakage current and conducting loss. In this work, we present a novel atomic layer deposition process to grow epitaxially $\text{Mg}_x\text{Ca}_{1-x}\text{O}$ dielectric layers on 4H-SiC(0001) and $\beta\text{-Ga}_2\text{O}_3(\bar{2}01)$ substrates. By tuning the composition of $\text{Mg}_x\text{Ca}_{1-x}\text{O}$ toward the substrate lattice constant, better interfacial epitaxy can be achieved. The interfacial and epitaxy qualities were investigated and confirmed by cross-sectional transmission electron microscopy and X-ray diffraction studies. $\text{Mg}_{0.72}\text{Ca}_{0.28}\text{O}$ film showed the highest epitaxy quality on 4H-SiC(0001) because of its closest lattice match with the substrate. Meanwhile, highly textured $\text{Mg}_{0.25}\text{Ca}_{0.75}\text{O}$ films can be grown on $\beta\text{-Ga}_2\text{O}_3(\bar{2}01)$ with a preferred orientation of (111).

Introduction

With the rapid expansion of semiconductor industry, power transistors are widely applied in the fast-growing fields such as electrical vehicles, solar energy, and giant data centers [1, 2]. The most important figure of merit (FOM) for high frequency power transistors is $R_{\text{on}} \times Q_g$ that characterizes the energy loss for high frequency operation [3, 4, 5]. Here, R_{on} is the resistance during “on” state, which is proportional to the conducting loss. Q_g stands for the total gate charge, which represents the loss during switching operations. Silicon-based power devices cannot fulfill the required high FOM in high-power applications because its low breakdown electric field requires a larger gate to drain distance, which would increase the R_{on} substantially and, thus, increase the total energy loss [6, 7, 8].

Wide band gap semiconductors, including SiC, Ga_2O_3 , and GaN, can overcome this challenge because their high breakdown electric field facilitates a smaller gate to drain distance, so that R_{on} can be reduced proportionally. Furthermore, GaN-based

high electron mobility transistors (HEMTs) can further reduce R_{on} by introducing 2-dimensional electron gas (2DEG). However, the application of GaN-based HEMT arouses safety concerns for power electronic devices because of its intrinsically normally-on feature [9]. The current commercially available normally-off GaN HEMT devices are achieved by adopting the so called “cascode” configuration. This configuration consists of the series connection of a low-voltage normally-off Si-based metal oxide semiconductor field effect transistor (MOSFET) with a high voltage normally-on GaN HEMT [10]. Other strategies to achieve normally-off GaN HEMT, such as p-Gate [11], fluorine gate [12], and gate recess [13, 14], were proposed and received numerous attention from both academia and industry. However, their complicated fabrication process and low reliability prevent them from mass industrial-level production. Therefore, the intrinsically normally-off SiC and Ga_2O_3 power transistors would be more favorable in industrial applications because of their safety nature.

A key challenge for SiC and Ga₂O₃ devices is the lack of a suitable dielectric material that can both reduce the gate leakage and the interfacial defects [15]. High gate leakage current would deteriorate the device reliability and increase the on-state loss. Also, interfacial defects under the gate electrode can substantially increase switching loss by trapping electrons that in turn increase Q_g . Moreover, charged defects can also scatter electrons in the channel so that R_{on} is increased as well.

SiC can form a native oxide (SiO₂) with one or two order of magnitude higher interfacial defect density than the SiO₂/Si interface because of the incomplete oxidation of carbon [16, 17]. Moreover, the low dielectric constant (3.9) of SiO₂ limits the maximum safe operating electric field, and the high breakdown field of SiC cannot be used fully [18]. As for β-Ga₂O₃ transistors, Schottky gate structure [19, 20] was used to form metal–semiconductor field effect transistor (MESFET). This type of structure has a nature of leaky gate that prevents high efficiency device operation and renders a low on/off ratio. HfO₂ [21], SiO₂ [22], and Al₂O₃ [23, 24] had been proposed as the gate dielectric to reduce the gate leakage currents. However, very few dielectric materials had been proposed to achieve a very high-quality interface along with very low leakage [25].

Both MgO and CaO have relatively high dielectric constants (MgO 9.8, CaO 11.8) and relatively large band gaps (both 7–8 eV) compared with SiC (3.3 eV) and Ga₂O₃ (4.5–4.9 eV) and, thus, might be suitable gate oxides for wide band gap semiconductors. Recently, our group has demonstrated that an epitaxial Mg_xCa_{1-x}O film can be grown on GaN(0001) surfaces using a suitable ALD process, achieving low interfacial defect density and high electrical performance [26]. We demonstrated a low defect density interface between semiconductor substrates and a lattice matched epitaxial gate dielectric material. Q_g can be effectively minimized with this reduced interfacial defect density, and therefore, the overall device loss was reduced. Moreover, because there are few grain boundaries to serve as the leakage pathways, gate leakage loss was also reduced. 4H SiC has a similar hexagonal symmetry on the (0001) surface with the GaN(0001). With only –4% of lattice mismatch with GaN, SiC is widely used as the epitaxial growth substrate for GaN in LED industry. Bhuiyan et al. also demonstrated that Mg_xCa_{1-x}O is a promising radiation-tolerant gate dielectric material for GaN-based MOSHEMTs [27]. β-Ga₂O₃ on the other hand has a monolithic structure that does not exactly match the hexagonal symmetry of the rock salt Mg_xCa_{1-x}O(111) surface. But its ($\bar{2}01$) surface has a structure similar to a hexagonal structure, which makes it also suitable as the substrate for GaN epitaxial growth [28, 29]. Therefore, it is highly possible to grow Mg_xCa_{1-x}O epitaxially on the SiC(0001) and β-Ga₂O₃($\bar{2}01$) surfaces which are close to GaN(0001).

Moreover, as shown in Fig. 1, the SiC lattice sizes lie between those of MgO and CaO lattices. Therefore, by tuning the composition of Mg_xCa_{1-x}O, a lattice match with SiC substrates can be achieved. According to Vegard's Law [30], a 76% Mg and 24% Ca oxide mixture can achieve a lattice match with SiC with an epitaxy relation of $(111)_{Mg_xCa_{1-x}O} // (0001)_{SiC}$. In the meantime, because β-Ga₂O₃($\bar{2}01$) surface is similar to GaN(0001) surface, it is anticipated to be lattice match with a composition near Mg_{0.25}Ca_{0.75}O. Epitaxial Mg_{0.75}Ca_{0.25}O grown by molecular beam epitaxy (MBE) on SiC has been reported as an alternative dielectric oxide [31]. Moreover, epitaxial GaN has been reported to be grown on β-Ga₂O₃ ($\bar{2}01$) surface by MBE [32]. Therefore, MBE-grown dielectrics can be expected for Ga₂O₃ substrates as well. Measurements on HEMTs with MBE-fabricated MgCaO insulators showed improved gate-lag [33]. However, MBE endures problems such as low industrial compatibility due to ultra-high vacuum requirements and high cost. Furthermore, MBE is not applicable to large substrates needed for cost-effective industrial processing. Thus, a more scalable and lower cost method to deposit epitaxial Mg_xCa_{1-x}O is highly desirable. Atomic layer deposition (ALD) is a well-established method to achieve films with high uniformity and highly controllable precision. Moreover, ALD technique is more cost effective and industrial compatible compared with MBE, providing potential way to achieve precisely controlled and high-quality dielectric films. Thus, in this study, we focused on applying the ALD process to grow epitaxially Mg_xCa_{1-x}O on SiC(0001) and β-Ga₂O₃($\bar{2}01$) substrates.

Results and discussions

Epitaxial growth of Mg_xCa_{1-x}O on SiC

SiC has two primary polytypes for semiconductor applications, 4H and 6H, respectively. Both 4H and 6H are hexagonal, and each has a similar (0001) surface structure and a relatively small lattice mismatch to GaN, –3.8% and –3.5%, respectively. Traditionally, 4–8 degrees of off-axis SiC were grown with liquid or vapor phase epitaxial growth because the higher density of surface steps can improve the growth quality [34]. However, Hijikata et al. had pointed out that the lower angle of off-axis SiC can effectively reduce the interfacial traps [35]. In our case, the surface symmetry of off-angle SiC also does not match with the hexagonal structure of rock salt (111) surface. Therefore, an on-axis SiC 4H is selected as the substrate. To perform a comprehensive study on how lattice mismatch influences epitaxy growth, films with three compositions such as pure MgO, Mg_{0.72}Ca_{0.28}O, and Mg_{0.51}Ca_{0.49}O were investigated. According to Vegard's law, as shown in Fig. 1(b), the SiC lattice matches with Mg_{0.72}Ca_{0.28}O is expected to have best epitaxy quality. The substrate surface pretreatments and ALD

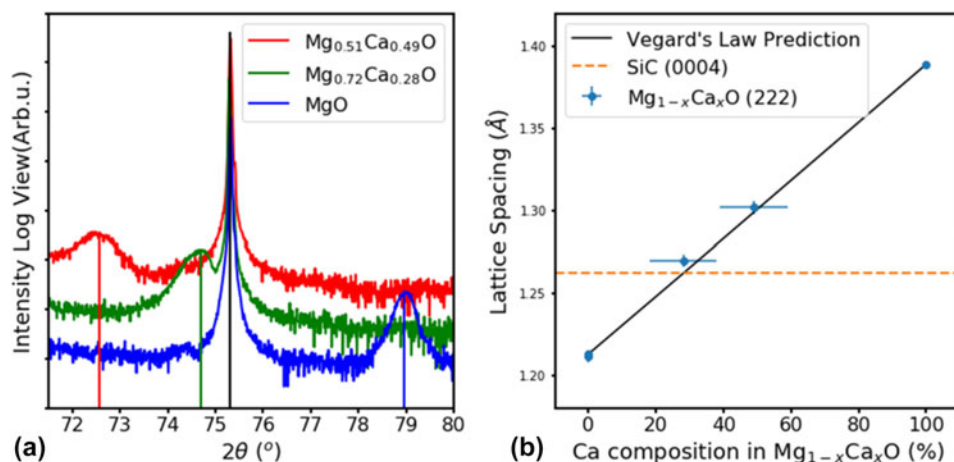


Figure 1: (a) 2θ - ω scans of three $Mg_xCa_{1-x}O/SiC$ samples. (b) Lattice constant of $Mg_xCa_{1-x}O$ with respect to Ca content in the film. Comparing SiC(0004) lattice with $Mg_xCa_{1-x}O(222)$ lattice, it shows that the $Mg_{0.72}Ca_{0.28}O$ has the smallest lattice mismatch with SiC.

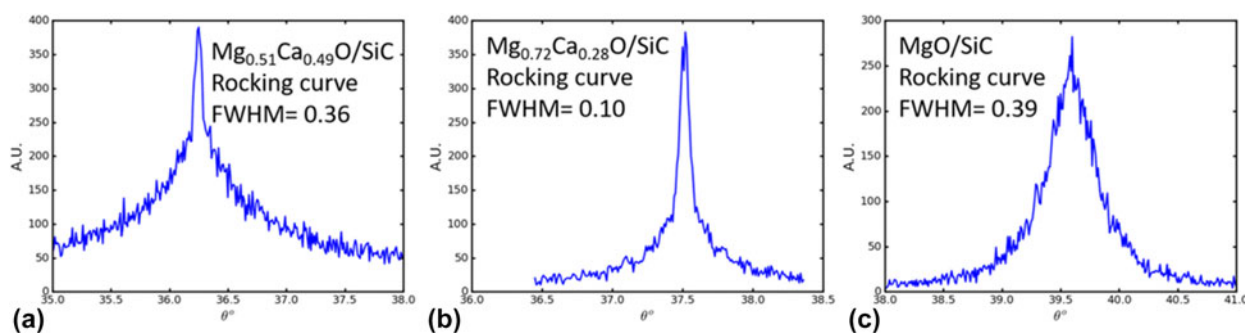


Figure 2: Rocking curves of $Mg_xCa_{1-x}O/4H-SiC(0001)$. (a) Rocking curve of $Mg_{0.51}Ca_{0.49}O/SiC$ at $2\theta = 72.55^\circ$. (b) Rocking curve of $Mg_{0.72}Ca_{0.28}O/SiC$ at $2\theta = 74.70^\circ$. (c) Rocking curve of MgO/SiC at $2\theta = 78.96^\circ$.

$Mg_xCa_{1-x}O$ deposition were performed with the conditions described in the Experiments and Methods section. X-ray diffraction (XRD) was conducted to further confirm the lattice matching of the $Mg_xCa_{1-x}O$ and SiC substrate. Figure 1(a) shows 2θ - ω scans of three $Mg_xCa_{1-x}O/SiC$ samples. 2θ - ω results show that the lattice mismatch of $Mg_{0.51}Ca_{0.49}O$ and $Mg_{0.72}Ca_{0.28}O$ are +3.2% and +0.7%, and -3.9%, respectively. It is clear that the $Mg_{0.72}Ca_{0.28}O$ has the closest match with SiC. This result is further verified by the corresponding rocking curves shown in Fig. 2. The narrower rocking curve of $Mg_{0.72}Ca_{0.28}O/SiC$ (FWHM = 0.1°) than $Mg_{0.51}Ca_{0.49}O/SiC$ (FWHM = 0.36°) and MgO/SiC (FWHM = 0.39°) indicates the former has the highest epitaxial quality. The fact that the lattice constants of $Mg_xCa_{1-x}O$ films are very close to the corresponding Vegard's law prediction, indicating that there is little stress. The extra sharpness of the $Mg_{0.51}Ca_{0.49}O$ and $Mg_{0.72}Ca_{0.28}O$'s rocking curve might be due to the relaxation of the top layer of the film.

Ren et al. had pointed out that the drawback of this ternary dielectric system is the large difference in the ionic radius between Mg and Ca causing severe immiscibility [31, 36],

particularly at high temperature. As a result, solid-solution CaO-MgO would be difficult to synthesize using bulk techniques because the two phases are immiscible over the entire composition range. However, the use of ALD as a film growth technique often allows for the formation of metastable phases, overcoming miscibility issues due to the unique self-terminating nature of growth. According to our research, $Mg_xCa_{1-x}O$ ternaries are kinetically stable as solid solution films over the entire compositional range when grown at a remarkably low temperature of 300 °C. The absence of CaO and MgO peaks in the XRD pattern also confirmed that there is no phase separation.

Cross-sectional transmission electron microscopy (TEM) was used to study the interfacial region of this epitaxial structure. Like the typical GaN cross-sectional TEM, SiC also shows a three atomic line periodicity pattern in the vertical direction because of its hexagonal structure [26]. Therefore, the interface between the substrate and $Mg_xCa_{1-x}O$ film can be determined by where this three-line periodicity discontinued. A sharp interface without any interfacial layer can be seen in Figs. 3(a) and 3(c). The traditional oxidized SiO₂ dielectric on

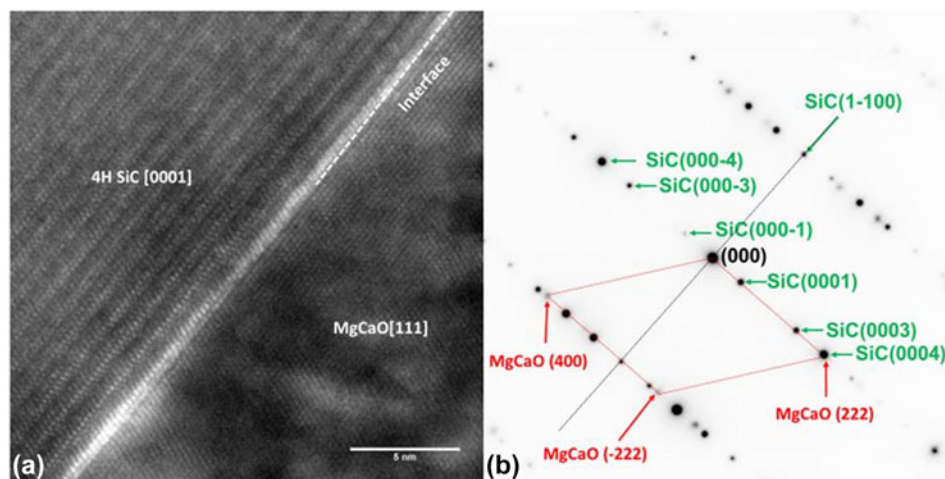


Figure 3: TEM cross section of $Mg_{0.72}Ca_{0.28}O/SiC(0001)$. (a) Cross-sectional TEM image. (b) Diffraction pattern of the (a) region. The zone axis of the SiC is $[11\bar{2}0]$ and for $Mg_{0.72}Ca_{0.28}O$ is $[011]$.

SiC is caused by the roughened interface [37]. In the ALD-grown epitaxial $Mg_xCa_{1-x}O$ on SiC, the pristine interface is preserved. The very well-defined diffraction spots in (b) also confirm the high epitaxial quality of the film. Twinning formation is common in crystalline films, with 180° mirror images having almost identical formation energy as shown in the $Mg_{0.72}Ca_{0.28}O$ left-right symmetric diffraction pattern [38, 39]. Moreover, from the diffraction pattern, the zone axis of the SiC substrate in these TEM images is $[11\bar{2}0]$, and the film zone axis can be determined as $[0\bar{1}1]$. Therefore, the epitaxial relation between the film and substrate is $Mg_{0.72}Ca_{0.28}O(111) \times [0\bar{1}1]//SiC(0001) \times [11\bar{2}0]$. Theoretical studies on $Mg_xCa_{1-x}O$ ternary systems also predicted a CsCl phase is possible [40]. But the TEM diffraction pattern clearly showed that there is no phase other than rock salt and also no phase separation is observed.

In summary, the XRD and TEM studies confirmed that the ALD $Mg_xCa_{1-x}O$ can be grown epitaxially on 4H-SiC (0001) substrates. $Mg_{0.72}Ca_{0.28}O$ shows the best lattice match with a +0.7% mismatch with the SiC substrate. The rocking curve also confirms that this smaller lattice match has a better epitaxial quality than the samples with larger mismatch.

Epitaxial growth of $Mg_xCa_{1-x}O$ on Ga_2O_3

Although $\beta-Ga_2O_3$ has a monoclinic crystal structure and does not have hexagonal symmetry on any crystal face, the O atoms on $\beta-Ga_2O_3(\bar{2}01)$ surface are roughly lined up on the same plane [Fig. 4(a)] and formed a nearly hexagonal structure from the top view [Fig. 4(b)]. Moreover, the distance between these O atoms are close to the distance between the N atoms on GaN(0001). Kitamura et al. had demonstrated that an epitaxial GaN can be grown on $\beta-Ga_2O_3$, with a lattice mismatch as small as 2.6%. Therefore, it is possible to create an epitaxial

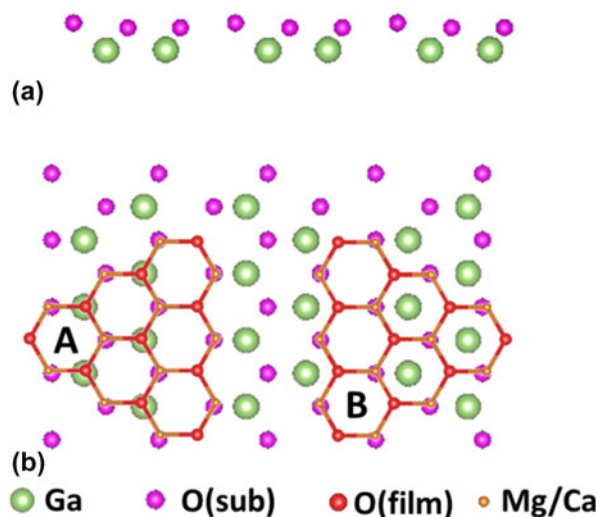


Figure 4: (a) Side view of $\beta-Ga_2O_3(\bar{2}01)$ lattice. (b) Top view of $Mg_xCa_{1-x}O(111)/\beta-Ga_2O_3(\bar{2}01)$.

growth of $Mg_xCa_{1-x}O$ on a $\beta-Ga_2O_3(\bar{2}01)$ surface as shown in Fig. 4.

As shown in Fig. 4(b), there are also two different possible orientations denoted as A and B. In both cases, Mg/Ca atoms are always stacking over substrate O atoms. In case A, half of film oxygen atoms are stacking over Ga atoms and the other half are on the vacancies surrounded by three oxygen atoms from the substrate. On the other hand, in case B, the film oxygen atoms are all on top of the vacancies surrounded by three oxygen atoms from the substrate. Thus, a ϕ scan is used to determine which orientation is achieved with ALD growth. The $Mg_xCa_{1-x}O(200)$ peak and $Ga_2O_3(202)$ peak are close in both 2θ and ω offset in $Mg_xCa_{1-x}O(111)/\beta-Ga_2O_3(\bar{2}01)$ structure. Therefore, a ϕ scan is set for scanning based on the position of $Ga_2O_3(202)$ peak at $\psi 54^\circ$ and $2\theta 38.62^\circ$.

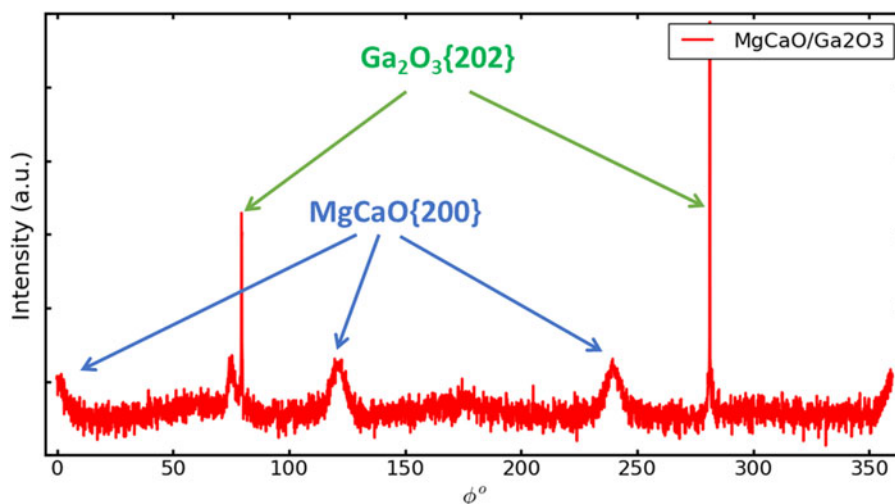


Figure 5: ϕ scan of $\text{Mg}_{0.25}\text{Ca}_{0.75}\text{O}/\text{Ga}_2\text{O}_3(\bar{2}01)$.

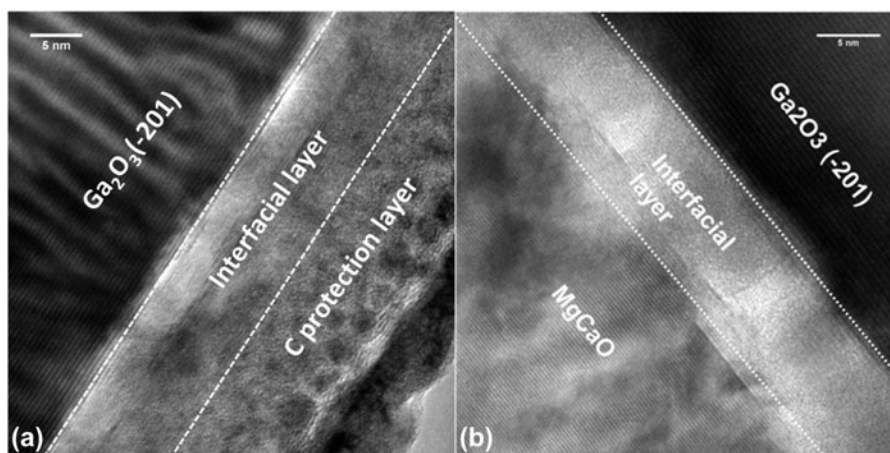


Figure 6: Cross-sectional TEM of (a) Piranha-treated bare Ga_2O_3 surface and (b) $\text{Mg}_{0.25}\text{Ca}_{0.75}\text{O}$ on Piranha-treated Ga_2O_3 .

Figure 5 demonstrates the ϕ scan of $\text{Mg}_{0.25}\text{Ca}_{0.75}\text{O}/\beta\text{-Ga}_2\text{O}_3$, which has a 3-fold symmetry, confirming that there is only one in-plane orientation existing in the film. Furthermore, the substrate (202) peak does not overlap with the film (200) peaks in ϕ scan, indicating that the film has a B-type orientation as shown in previously in Fig. 4(b).

To achieve epitaxial growth of $\text{Mg}_x\text{Ca}_{1-x}\text{O}$ on $\beta\text{-Ga}_2\text{O}_3$ substrates, ultra-clean surfaces of $\beta\text{-Ga}_2\text{O}_3$ substrate are needed. However, $\beta\text{-Ga}_2\text{O}_3$ is unstable under both acidic and basic conditions. Therefore, its surface treatment is very challenging. Some reports show that Piranha and buffered oxide etch (BOE) treatments are effective to prepare the $\beta\text{-Ga}_2\text{O}_3$ surface [41]. In this study, both pretreatments are used for comparison.

The cross-sectional TEM images of $\text{Mg}_{0.25}\text{Ca}_{0.75}\text{O}$ grown on both Piranha and BOE treated $\beta\text{-Ga}_2\text{O}_3(\bar{2}01)$ are shown in Figs. 6 and 7, respectively. The Piranha treatment is a common method for $\beta\text{-Ga}_2\text{O}_3$ surface cleaning used in a few Refs. [42, 43].

Although benefiting electrical performance in the literature, the Piranha-treated sample exhibits a 10 nm amorphous-like interfacial layer. This interfacial layer may be from the hydroxylation of $\beta\text{-Ga}_2\text{O}_3$ in the acid pretreatment.

In the meantime, as shown in Fig. 7(a), the 30 s BOE-treated sample (1:6 original diluted with 5 times volume of water) has only a 2 nm interfacial layer. This is a substantial improvement compared with the Piranha-treated substrate. However, severe delamination has been observed on the edge of $\beta\text{-Ga}_2\text{O}_3$ substrates, indicating surface damage caused by BOE treatment. In Fig. 7(b), the diffraction pattern of both the film and substrate indicates an epitaxial relationship to be $\text{Mg}_x\text{Ca}_{1-x}\text{O}[0\bar{1}1] \times (111)//\beta\text{-Ga}_2\text{O}_3[010] \times (\bar{2}01)$. In addition, the diffraction pattern in Fig. 7(b) indicates a highly textured film, with some misoriented crystal phases.

XRD was then carried out to further investigate the epitaxial growth quality of $\text{Mg}_{0.25}\text{Ca}_{0.75}\text{O}/\beta\text{-Ga}_2\text{O}_3$. The full 2θ - ω scan of $\text{Mg}_{0.25}\text{Ca}_{0.75}\text{O}/\beta\text{-Ga}_2\text{O}_3$ is demonstrated in Fig. 8.

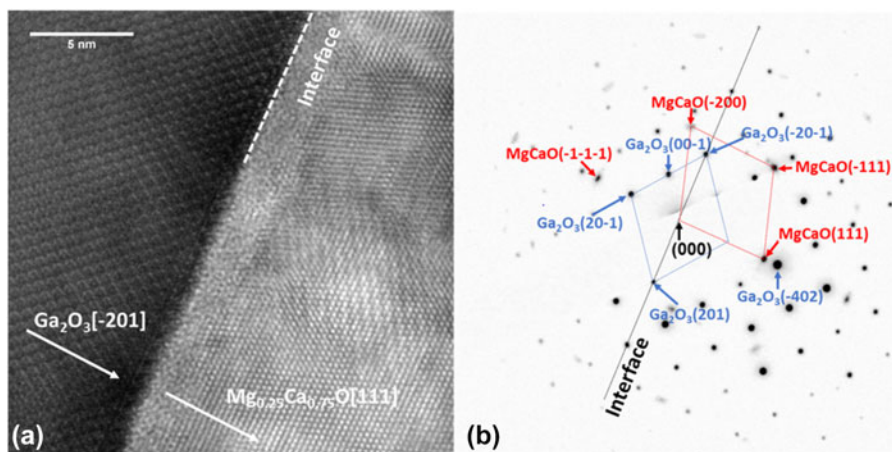


Figure 7: TEM of $\text{Mg}_{0.25}\text{Ca}_{0.75}\text{O}/\text{Ga}_2\text{O}_3(\bar{2}01)$ after BOE surface treatment. (a) High resolution image of $\text{Mg}_{0.25}\text{Ca}_{0.75}\text{O}$ and Ga_2O_3 interface, a 2 nm interfacial layer is visible. (b) Diffraction pattern. The zone axis of $\beta\text{-Ga}_2\text{O}_3$ is $[010]$. The main diffraction spots of $\text{Mg}_{0.25}\text{Ca}_{0.75}\text{O}$ indicate that the zone axis of the film is $[0\bar{1}1]$. The stray diffraction spots from $\text{Mg}_{0.25}\text{Ca}_{0.75}\text{O}$ are indicating that the film is highly textured with some misoriented crystal phases.

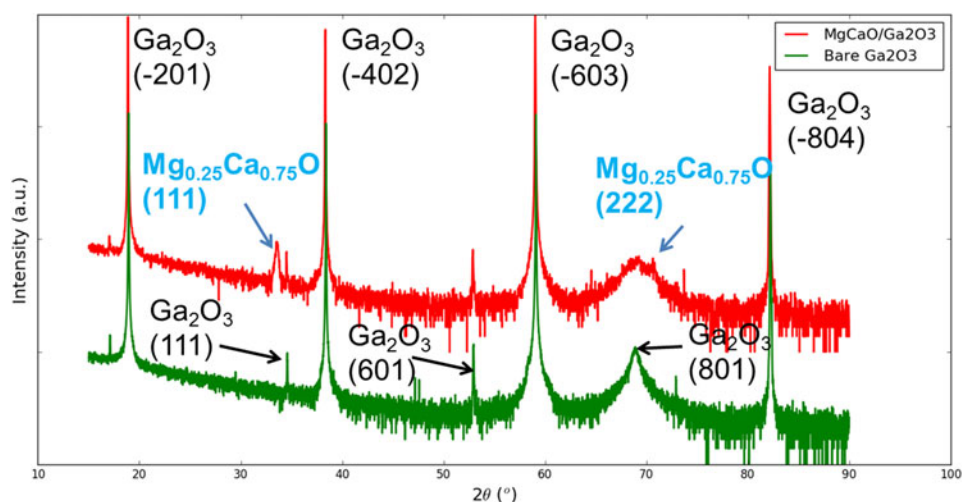


Figure 8: $2\theta\text{-}\omega$ of $\text{Mg}_{0.25}\text{Ca}_{0.75}\text{O}/\text{Ga}_2\text{O}_3$ and bare Ga_2O_3 .

The existence of (111) and (222) peaks of $\text{Mg}_{0.25}\text{Ca}_{0.75}\text{O}$ indicates the film has a preferred (111) orientation. The (222) peak of the film is not as obvious as (111) because it is overlapping with (801) peak from the substrate. The $\beta\text{-Ga}_2\text{O}_3(111)$, (601), and (801) peaks indicate that the substrate contains other small crystals with disordered orientations.

In summary, highly textured $\text{Mg}_{0.25}\text{Ca}_{0.75}\text{O}$ can be grown on $\beta\text{-Ga}_2\text{O}_3(\bar{2}01)$ with a preferred orientation of (111). The dielectric films are highly textured rather than epitaxial mainly because $\beta\text{-Ga}_2\text{O}_3(\bar{2}01)$ lattice is not perfectly hexagonal, which can introduce mismatch to the film (111) surface. Another minor cause might be the nonideal surface pretreatments. The $\beta\text{-Ga}_2\text{O}_3$ surface pretreatment has a profound effect on the interfacial property. BOE treatment can effectively reduce the interfacial layer thickness damages of the substrate to some extent.

Conclusion

In this work, we demonstrated for the first time that epitaxial and highly textured $\text{Mg}_x\text{Ca}_{1-x}\text{O}$ can be grown on $\text{SiC}(0001)$ and $\beta\text{-Ga}_2\text{O}_3(\bar{2}01)$ with an ALD process. Because $\text{SiC}(0001)$ has hexagonal symmetry, $\text{Mg}_x\text{Ca}_{1-x}\text{O}$ can be grown epitaxially on it. The closest lattice matching $\text{Mg}_{0.72}\text{Ca}_{0.28}\text{O}$ showed the highest epitaxy quality in an XRD rocking scan. Therefore, it has the greatest potential to achieve superior dielectric properties and should be the best candidate for device applications. In the meantime, highly textured $\text{Mg}_{0.25}\text{Ca}_{0.75}\text{O}$ can be grown on $\beta\text{-Ga}_2\text{O}_3(\bar{2}01)$ with a preferred orientation of (111). The $\text{Mg}_{0.25}\text{Ca}_{0.75}\text{O}$ film on $\beta\text{-Ga}_2\text{O}_3(\bar{2}01)$ is textured instead of epitaxial because the substrate surface is not perfectly matching the hexagonal symmetry of the film (111) surface. The crystal orientation relationship between $\text{Mg}_x\text{Ca}_{1-x}\text{O}$ and $\beta\text{-Ga}_2\text{O}_3$ was determined by XRD scans. Cross-sectional TEM showed that

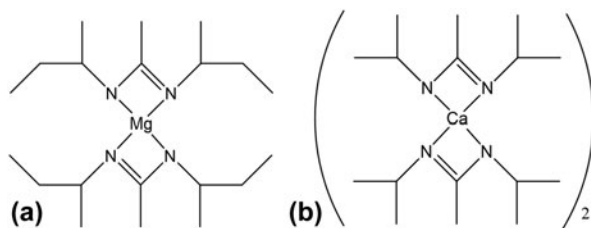


Figure 9: Structures of the metal precursors. (a) bis(*N,N'*-di-*sec*-butylacetaminato)magnesium and (b) bis(*N,N'*-diisopropylacetamidinato)calcium(II) dimer.

BOE treatment can effectively reduce the thickness of amorphous β -Ga₂O₃ top layer compared with Piranha treatment.

Experiments and methods

Substrate pretreatments

Both SiC and Ga₂O₃ substrates were purchased from MTI Corp. Surface pretreatments of substrates are crucial to the success of epitaxial growth of Mg_xCa_{1-x}O films because epitaxy is very sensitive to interfacial conditions. SiC substrates were soaked and rinsed 5 min in isopropanol and acetone and then methanol was conducted subsequently as basic surface cleaning. Then a 5 min UV-ozone and 30 s buffered oxide etch (BOE; 1:6 original diluted with 5 times volume water) were followed to remove the organic contaminants and surface oxide. In the case of Ga₂O₃, same surface pretreatment procedures were carried out for one batch of substrates. As a comparison experiment, the final step of 30 s BOE etch was replaced with 30 s Piranha (a mixture of 3:1 sulfuric acid and hydrogen peroxide) etch for the other batch of substrates.

Mg_xCa_{1-x}O film growth

ALD of Mg_xCa_{1-x}O was carried out in a home-built tubular reactor. Mg_xCa_{1-x}O films were obtained by alternating doses of calcium, magnesium, and oxygen sources, where bis(*N,N'*-diisopropylacetamidinato)calcium(II) dimer [13], bis(*N,N'*-di-*sec*-butylacetamidinato)magnesium, and H₂O were used as precursors, respectively. Structural formulas for Mg and Ca precursors are shown in Fig. 9. The Mg precursor is kept at 110 °C, whereas the Ca precursor is kept at 140 °C to provide enough vapor pressure. H₂O is kept at room temperature. During the deposition, the samples/substrates are placed on the substrate holder kept at 310 °C under vacuum. In each dosing cycle, either the Mg or Ca precursor is dosed into the reaction chamber and then purged for 30 s. Then H₂O vapor is dosed and purged. Four different precursor dosing ratios, namely, Mg only, Mg:Ca = 1:1, Mg:Ca = 1:2, and Mg:Ca = 1:3, were used. The dosing sequence is repeated for the corresponding number of Mg cycles, then Ca cycles. Because of the large size of the ligands, each metal cycle cannot fully cover one atomic layer. Therefore, the alternating Mg and Ca cycles can give a uniform film

instead of layered structure. The compositions of the resulting films were determined by RBS (Rutherford Backscattering Spectrometry) to be MgO, Mg_{0.72}Ca_{0.28}O, Mg_{0.51}Ca_{0.49}O, and Mg_{0.25}Ca_{0.75}O, respectively. The film growth rates with different dosing ratios and the corresponding compositions are summarized in the literature published by our group [26]. The total ALD Mg_xCa_{1-x}O film thickness is 40 nm for further characterization. Because MgO and CaO are both reactive with moisture, a 5 nm of Al₂O₃ is grown in situ on top of Mg_xCa_{1-x}O for both SiC and β -Ga₂O₃ substrates to prevent water in air from permeation into the epitaxial film during XRD and TEM characterization.

Film epitaxy characterizations

Cross-sectional TEM and diffraction patterns were conducted on Mg_xCa_{1-x}O/SiC and Mg_xCa_{1-x}O/Ga₂O₃ samples with the Joel 2100 High resolution TEM in Harvard CNS (Center for Nanoscale Systems). The TEM samples were beforehand prepared with an FEI Helios 660 FIB (focused ion beam) system and then cleaned with 500 eV Ar ion beam with a Fischione NanoMill 1040 in Harvard CNS. XRD measurements were carried out in the Bruker D8 high resolution XRD facility in Harvard CCB (Chemistry & Chemical Biology Department) X-ray Laboratory. The ϕ scan of Mg_xCa_{1-x}O is achieved by first determining the 2θ and ω angle of Mg_xCa_{1-x}O (200) position with asymmetric 2θ - ω scan and rocking scan. Then a ϕ scan is conducted by collecting the Mg_xCa_{1-x}O (200) peak while rotating the sample stage.

Author contributions

The manuscript was written through contributions of all authors. X.B.L. and X.G. contributed equally.

Acknowledgments

This work was supported by the US National Science Foundation grant 1764338, the US Office of Naval Research contract N00014-10-1-0937, the US Department of Energy—Office of Science contract DE-AC36-08GO28308, and the Charles Stark Draper Laboratory, Inc. contract SC001-0000000950. This work was performed in part at the Harvard University Center for Nanoscale Systems (CNS), a member of the National Nanotechnology Coordinated Infrastructure Network (NNCI), which is supported by the National Science Foundation under NSF ECCS Award No. 1541959.

Supplementary material

To view supplementary material for this article, please visit <https://doi.org/10.1557/jmr.2019.376>.

References

- J.B. Casady and R.W. Johnson:** Status of silicon carbide (SiC) as a wide-bandgap semiconductor for high-temperature applications: A review. *Solid-State Electron.* **39**, 1409 (1996).
- S. Fujita:** Wide-bandgap semiconductor materials: For their full bloom. *Jpn. J. Appl. Phys.* **54**, 030101 (2015).
- Y. Zhang, M. Sun, J. Perozek, Z. Liu, A. Zubair, D. Piedra, N. Chowdhury, X. Gao, K. Shepard, and T. Palacios:** Large-area 1.2-kV GaN vertical power FinFETs with a record switching figure of merit. *IEEE Electron Device Lett.* **40**, 75 (2018).
- K. Shenai:** The figure of merit of a semiconductor power electronics switch. *IEEE Trans. Electron Devices* **65**, 4216 (2018).
- H. Wang, J. Wei, R. Xie, C. Liu, G. Tang, and K.J. Chen:** Maximizing the performance of 650-V p-GaN gate HEMTs: Dynamic RON characterization and circuit design considerations. *IEEE Trans. Power Electron.* **32**, 5539 (2016).
- T.P. Chow and R. Tyagi:** Wide bandgap compound semiconductors for superior high-voltage power devices. In [1993] *Proceedings of the 5th International Symposium on Power Semiconductor Devices and ICs* (IEEE, Zurich, 1993); p. 84.
- J. Millán, P. Godignon, X. Perpiñà, A. Pérez-Tomás, and J. Rebollo:** A survey of wide bandgap power semiconductor devices. *IEEE Trans. Power Electron.* **29**, 2155 (2013).
- M.N. Yoder:** Wide bandgap semiconductor materials and devices. *IEEE Trans. Electron Devices* **43**, 1633 (1996).
- M. Östling, R. Ghandi, and C-M. Zetterling:** SiC power devices—Present status, applications and future perspective. In *2011 IEEE 23rd International Symposium on Power Semiconductor Devices and ICs* (IEEE, Zurich, 2011); p. 10.
- F. Roccaforte, G. Greco, P. Fiorenza, and F. Iucolano:** An overview of normally-off GaN-based high electron mobility transistors. *Materials* **12**, 1599 (2019).
- E.A. Jones, F.F. Wang, and D. Costinett:** Review of commercial GaN power devices and GaN-based converter design challenges. *IEEE Trans. Emerg. Sel. Topics Power Electron.* **4**, 707 (2016).
- Y. Cai, Y. Zhou, K.J. Chen, and K.M. Lau:** High-performance enhancement-mode AlGaIn/GaN HEMTs using fluoride-based plasma treatment. *IEEE Electron Device Lett.* **26**, 435 (2005).
- W. Saito, Y. Takada, M. Kuraguchi, K. Tsuda, and I. Omura:** Recessed-gate structure approach toward normally off high-voltage AlGaIn/GaN HEMT for power electronics applications. *IEEE Trans. Electron Devices* **53**, 356 (2006).
- W. Lanford, T. Tanaka, Y. Otoki, and I. Adesida:** Recessed-gate enhancement-mode GaN HEMT with high threshold voltage. *Electron. Lett.* **41**, 449 (2005).
- G. Liu, B.R. Tuttle, and S. Dhar:** Silicon carbide: A unique platform for metal-oxide-semiconductor physics. *Appl. Phys. Rev.* **2**, 021307 (2015).
- K. Gao, T. Seyller, L. Ley, F. Ciobanu, G. Pensl, A. Tadich, J. Riley, and R. Leckey:** Al₂O₃ prepared by atomic layer deposition as gate dielectric on 6H-SiC(0001). *Appl. Phys. Lett.* **83**, 1830 (2003).
- V. Afanasev, M. Bassler, G. Pensl, and M. Schulz:** Intrinsic SiC/SiO₂ interface states. *Phys. Status Solidi B* **162**, 321 (1997).
- C.M. Tanner, Y-C. Perng, C. Frewin, S.E. Saddow, and J.P. Chang:** Electrical performance of Al₂O₃ gate dielectric films deposited by atomic layer deposition on 4H-SiC. *Appl. Phys. Lett.* **91**, 203510 (2007).
- M. Higashiwaki, K. Sasaki, A. Kuramata, T. Masui, and S. Yamakoshi:** Gallium oxide (Ga₂O₃) metal-semiconductor field-effect transistors on single-crystal β-Ga₂O₃(010) substrates. *Appl. Phys. Lett.* **100**, 013504 (2012).
- M. Higashiwaki, K. Sasaki, A. Kuramata, T. Masui, and S. Yamakoshi:** Development of gallium oxide power devices. *Phys. Status Solidi B* **211**, 21 (2014).
- M.J. Tadjer, N.A. Mahadik, V.D. Wheeler, E.R. Glaser, L. Ruppalt, A.D. Koehler, K.D. Hobart, C.R. Eddy, and F.J. Kub:** A (001) β-Ga₂O₃ MOSFET with +2.9 V threshold voltage and HfO₂ gate dielectric. *ECS J. Solid State Sci. Technol.* **5**, P468 (2016).
- K. Konishi, T. Kamimura, M.H. Wong, K. Sasaki, A. Kuramata, S. Yamakoshi, and M. Higashiwaki:** Large conduction band offset at SiO₂/β-Ga₂O₃ heterojunction determined by X-ray photoelectron spectroscopy. *Phys. Status Solidi B* **253**, 623 (2016).
- P.H. Carey IV, F. Ren, D.C. Hays, B. Gila, S. Pearton, S. Jang, and A. Kuramata:** Band alignment of Al₂O₃ with (201) β-Ga₂O₃. *Vacuum* **142**, 52 (2017).
- K.D. Chabak, N. Moser, A.J. Green, D.E. Walker, Jr., S.E. Tetlak, E. Heller, A. Crespo, R. Fitch, J.P. McCandless, and K. Leedy:** Enhancement-mode Ga₂O₃ wrap-gate fin field-effect transistors on native (100) β-Ga₂O₃ substrate with high breakdown voltage. *Appl. Phys. Lett.* **109**, 213501 (2016).
- M. Higashiwaki, K. Sasaki, T. Kamimura, M. Hoi Wong, D. Krishnamurthy, A. Kuramata, T. Masui, and S. Yamakoshi:** Depletion-mode Ga₂O₃ metal-oxide-semiconductor field-effect transistors on β-Ga₂O₃(010) substrates and temperature dependence of their device characteristics. *Appl. Phys. Lett.* **103**, 123511 (2013).
- X. Lou, H. Zhou, S.B. Kim, S. Alghamdi, X. Gong, J. Feng, X. Wang, P.D. Ye, and R.G. Gordon:** Epitaxial growth of Mg_xCa_{1-x}O on GaN by atomic layer deposition. *Nano Lett.* **16**, 7650 (2016).
- M.A. Bhuiyan, H. Zhou, S-J. Chang, X. Lou, X. Gong, R. Jiang, H. Gong, E.X. Zhang, C-H. Won, and J-W. Lim:** Total-ionizing-dose responses of GaN-based HEMTs with different channel thicknesses and MOSHEMTs with epitaxial MgCaO as gate dielectric. *IEEE Trans. Nucl. Sci.* **65**, 46 (2017).
- T-Y. Tsai, R-H. Horng, D-S. Wu, S-L. Ou, M-T. Hung, and H-H. Hsueh:** GaN epilayer grown on Ga₂O₃ sacrificial layer for chemical lift-off application. *Electrochem. Solid-State Lett.* **14**, H434 (2011).

29. E.G. Villora, K. Shimamura, K. Kitamura, K. Aoki, and T. Ujiie: Epitaxial relationship between wurtzite GaN and β -Ga₂O₃. *Appl. Phys. Lett.* **90**, 234102 (2007).
30. H. Morkoç: *Handbook of Nitride Semiconductors and Devices Vol. 1: Materias Properties, Physics and Growth* (Wiley-VCH Verlag GmbH & Co. KGaA, Weinheim, 2008).
31. D. Stodilka, A.P. Gerger, M. Hlad, P. Kumar, B.P. Gila, R. Singh, C.R. Abernathy, S.J. Pearton, and F. Ren: Alternative magnesium calcium oxide gate dielectric for silicon carbide MOS application. *MRS Proc.* **911**, 0911 (2006).
32. S. Ohira, N. Suzuki, H. Minami, K. Takahashi, T. Araki, and Y. Nanishi: Growth of hexagonal GaN films on the nitridated β -Ga₂O₃ substrates using RF-MBE. *Phys. Status Solidi C* **4**, 2306 (2007).
33. B. Gila, M. Hlad, A. Onstine, R. Frazier, G. Thaler, A. Herrero, E. Lambers, C. Abernathy, S. Pearton, and T. Anderson: Improved oxide passivation of AlGaN/GaN high electron mobility transistors. *Appl. Phys. Lett.* **87**, 163503 (2005).
34. T. Ueda, H. Nishino, and H. Matsunami: Crystal growth of SiC by step-controlled epitaxy. *J. Cryst. Growth* **104**, 695 (1990).
35. Y. Hijikata, H. Yaguchi, S. Yoshida, Y. Takata, K. Kobayashi, H. Nohira, and T. Hattori: Off-angle dependence of characteristics of 4H-SiC–oxide interfaces. In *Materials Science Forum*, Vol. **527** (Trans Tech Publications, Piscataway, 2006); p. 1003.
36. R. Doman, J. Barr, and R. McNally: AM alper. *J. Am. Ceram. Soc.* **46**, 314 (1963).
37. T. Hosoi, K. Konzono, Y. Uenishi, S. Mitani, Y. Nakano, T. Nakamura, T. Shimura, and H. Watanabe: Investigation of surface and interface morphology of thermally grown SiO₂ dielectrics on 4H-SiC(0001) substrates. In *Materials Science Forum*, Vol. **679** (Trans Tech Publications, Piscataway, 2011); p. 342.
38. N. Sridhar, J. Rickman, and D. Srolovitz: Twinning in thin films—II. Equilibrium microstructures. *Acta Mater.* **44**, 4097 (1996).
39. C.M. Tanner, M.F. Toney, J. Lu, H-O. Blom, M. Sawkar-Mathur, M.A. Tafesse, and J.P. Chang: Engineering epitaxial γ -Al₂O₃ gate dielectric films on 4H-SiC. *J. Appl. Phys.* **102**, 104112 (2007).
40. A. Srivastava, M. Chauhan, R. Singh, and R. Padegaonker: High pressure phase transitions in Mg_{1-x}Ca_xO: Theory. *Phys. Status Solidi B* **248**, 1901 (2011).
41. J. Yang, Z. Sparks, F. Ren, S.J. Pearton, and M. Tadjer: Effect of surface treatments on electrical properties of β -Ga₂O₃. *J. Vac. Sci. Technol., B: Nanotechnol. Microelectron.: Mater., Process., Meas., Phenom.* **36**, 061201 (2018).
42. A. Jayawardena, A.C. Ahyi, and S. Dhar: Analysis of temperature dependent forward characteristics of Ni/ β -Ga₂O₃ Schottky diodes. *Semicond. Sci. Technol.* **31**, 115002 (2016).
43. H. Zhou, M. Si, S. Alghamdi, G. Qiu, L. Yang, and D.Y. Peide: High-performance depletion/enhancement-ode β -Ga₂O₃ on insulator (GOOI) field-effect transistors with record drain currents of 600/450 mA/mm. *IEEE Electron Device Lett.* **38**, 103 (2016).